




Effects of extreme transverse deformation on the strength of UHMWPE single filaments for ballistic applications

Kevin Golovin¹  and Stuart Leigh Phoenix^{2,*} 

¹Department of Materials Science and Engineering, Cornell University, Ithaca, NY 14853, USA

²Sibley School of Mechanical and Aerospace Engineering, Cornell University, Ithaca, NY 14853, USA

Received: 15 February 2016

Accepted: 18 May 2016

Published online:

2 June 2016

© Springer Science+Business Media New York 2016

ABSTRACT

Fibers used in both soft and hard body armor have very high longitudinal tensile strength and stiffness, but differ drastically in their transverse mechanical properties. Glass and carbon fibers are stiff and brittle in the transverse direction and easily shatter upon projectile impact unless they are cushioned within a soft matrix to disperse the load. In contrast, aramid fibers (e.g., Kevlar 29 and Twaron) and ultra-high-molecular-weight polyethylene (UHMWPE) fibers (e.g., Dyneema and Spectra) have quasi-plastic transverse behavior, with a low yield strength, and thus tend to flatten upon projectile impact, yet retain much of their tensile load-carrying capability. Thus, these polymer fibers are especially suitable for ‘soft’ body armor consisting of stacked sheets or fabrics, whereas the former glass and carbon fibers are useful mainly when aligned in a strong polymer matrix to form a thick plate. In this work, we report on a study of the tensile mechanical properties of single UHMWPE fibers (i.e., single filaments) that have been transversely deformed from their original cylindrical shape to form thin flat micro-tapes with a width-to-thickness ratio of up to 60:1. The deformed, ribbon-like fibers show very high retention in fiber strength, though with increased variability resulting from locally induced defects. Because transverse deformation resulted in more than a factor of three increase in surface area per unit length, the stress transfer length necessary to fully load a fiber near a break was found also to decrease by the same factor, as the corresponding interfacial shear stress remained the same. A Weibull probability analysis revealed that the increase in variability in fiber strength was consistent with a more pronounced length effect. These changes in fiber strength properties were understood through an alteration of the crystalline domains within the fibers due to the extreme deformation.

Address correspondence to E-mail: slp6@cornell.edu

Introduction

High-strength, polymeric fibers in the form of multiple layers of woven fabrics or non-woven $[0^\circ/90^\circ/0^\circ/90^\circ]$ composite sheets are used in personnel body armor because of their ability to withstand the impact of both bullets and shrapnel [1–3]. For many applications, ultra-high-molecular-weight polyethylene (UHMWPE) fibers are the most effective of these materials because of their unique combination of very low density, very high strength, and high stiffness [3, 4]. When bundles of UHMWPE fibers are impacted transversely, collapse of the void space between the fibers directly under the projectile leads to local flattening and distortion of the parallel fiber alignment in and around the impact zone. This leads to uneven tensile stress and strain distribution among these fibers in a phenomenon called interference [5, 6]. The resulting distortion in strain reduces the effective bundle strength needed to sustain the tension waves emanating from the impact zone. The strength of a non-woven, composite sheet is also influenced by the ability of the matrix to transfer stress from broken to intact fibers through shear [7], since fibers fail at random locations. This ability is limited by the low surface energy of UHMWPE fibers, making it difficult to bond them to the matrix. The length scale of unloading of a broken fiber is longer by more than an order of magnitude compared to other fibers [8–11]. Tension testing of single UHMWPE filaments is problematic for the same reason. Unlike with other types of fibers, adhesive methods of gripping (where single filaments are bonded to thin cardboard tabs using an epoxy or a cyanoacrylate adhesive) often suffer from debonding and slippage, particularly for larger diameter fibers, and thus lack consistency [12–14]. This has led to the search for more reliable methods of clamping, and one particular method that has proved successful uses PMMA or polycarbonate inserts in metal clamps that permanently distort the cylindrical fiber into a flat ribbon in the clamp region [15, 16], thus increasing the surface area for developing shear tractions in gripping.

To improve matrix adhesion, surface modification of UHMWPE has been studied using plasma treatments [17–21], resin improvements [22], and fiber coatings [23]. Each method has reportedly resulted in an increase in the interfacial shear strength (IFSS), the maximum shear stress that can be supported at the

interface without the occurrence of debonding, but a subsequent decrease in fiber strength. Additional drawbacks to these approaches are the difficulty in scaling up the processes and their cost. Moreover, since the matrix in such composites supports negligible tension, the matrix volume fraction should be minimized while maintaining a void-free structure. Hot compaction is a method to reduce the necessary amount of matrix, where the fibers and matrix are transversely compressed at elevated temperatures to induce bonding and eliminate voids [24, 25]. However, hot-pressed laminates still contain 14–17 % matrix and can show a subsequent drop in strength from chain scission and crosslinking. An additional issue with hot-pressed laminates is the distortion of the fiber and its alignment at fiber crossovers, depending on the compaction pressure and temperature cycle [25].

In this work, we present a novel fiber alteration method, where single UHMWPE fibers are mechanically deformed by squeezing them between a cylindrical metal roller on a plate or by pulling them between two opposing rollers, thus producing extremely flat, ribbon-shaped fibers with rectangular cross-sections. Previously, aramid fibers (e.g., Kevlar-29) have been transversely deformed using a compression method to measure the transverse properties of the fibers [26, 27] and tension tests afterwards have revealed as much as 90 % strength retention. Here we deform originally round UHMWPE Dyneema filaments into micro-ribbons with aspect ratios (width/depth) as high as 60:1. This process could potentially lead to fibers that approach 100 % packing efficiency and could eliminate both interference effects from inter-fiber void space [6] and the deformable matrix that supports negligible tension. Moreover, the stress transfer length would be significantly decreased, thus potentially improving bundle strength characteristics [7].

Experimental

Dyneema[®] SK-76 fiber was obtained from DSM in the Netherlands in the form of a 1760 dtex yarn having a nominal strength of 35 cN/dtex (34 GPa). Single fibers (filaments), approximately 18 μm in diameter, were carefully separated from these yarns for purposes of transverse deformation, microscopy, and testing for strength retention. To tab specimens for

tension testing and pullout experiments, Z-Poxy, a 5-min set epoxy purchased from ZAP adhesives, was found to work well provided that a sufficient length of fiber was embedded in epoxy in the tab/clamp regions. After considerable study, an embedment length of at least 2.5 cm was found to be suitable.

Two methods for transverse deformation of the filaments were developed. The first method, denoted the “hand roll” approach, involved manual rolling a 50-mm-diameter, chrome-coated steel rod (McMaster-Carr, 6689T183) over and along multiple, parallel filaments taped down separately along a 5-cm-wide by 20-cm-long by 1.25-cm-thick aluminum plate. The process is illustrated schematically in Fig. 1 and the total vertical applied rolling force was about 50 kg. Prior to the experiments, the plate had been polished down to 0-grit roughness starting from 180-grit polishing pads (final mean roughness R_a of 20–50 nm [28]). The chrome-coated rod had a mirror-like finish and surface variation had a diameter tolerance of ± 0.04 mm over a 90 cm length. Several rolling passes were made over a period of about 3 min and using various rolling angles in an attempt to minimize the effects of diameter variations of the rod and to obtain fairly uniform aspect ratios of the resulting ribbon-like deformed filaments.

The second method, denoted the “machine roll” method, was designed to deform fibers more efficiently and consistently with respect to the appearance of surface anomalies, and is illustrated in Fig. 2. The same versions of chrome-coated steel rods were arranged so as to roll directly against each other without slippage while continuously drawing

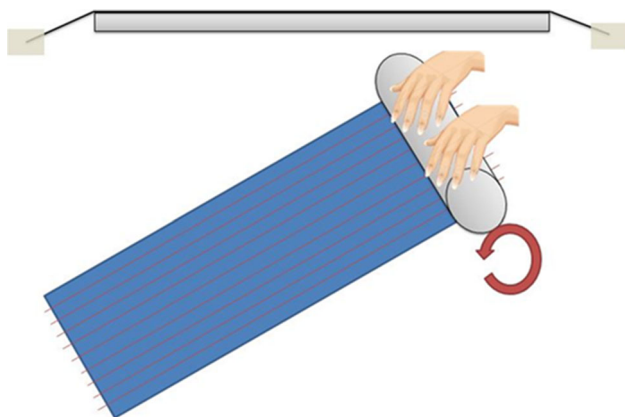


Figure 1 Sketch of the “hand” deformation method as well as a side view of single fibers taped down over the aluminum plate prior to rolling.

filaments between them through the machine at a 90° angle to the axes of the rods. Weights were hung from steel bars attached to each end of the top roller axle in order to apply a large vertical force to deform the fibers (Fig. 2d). A total vertical load of 82 kg was found to give consistent results in terms of cross-sectional aspect ratio of the deformed fibers. Once again, the extent and precision of fiber transverse deformation was limited somewhat by the diameter variation of the two mating rollers, and in contrast to the hand method, individual filaments were only subjected to a single deformation cycle when fed between the two rollers.

We let W and h be the deformed fiber’s width and height (thickness), respectively, which were measured optically using an Olympus BH-2 white-light microscope. We also let $\Phi = W/h$ be the deformed fiber’s aspect ratio. Initially, the fibers had a circular cross-section with diameter, D , measured optically to be 17.8 μm with a standard deviation of 1.7 μm . Assuming no volume change or significant permanent lengthening during the transverse deformation process, which was confirmed optically, we have $Wh = \pi D^2/4$, from which we calculate that

$$\Phi = \frac{4}{\pi} \left(\frac{W}{D} \right)^2. \tag{1}$$

For both deformation methods, a sample size of $N \geq 40$ individual fibers was used.

Deformed single fibers were subjected to tension tests using an Instron 1125 test machine at the gauge lengths of 1 and 10 cm. Pristine single fibers were also tension tested at the gauge lengths of 5, 10, and 30 cm using similar sample sizes. All filament specimens were fully bonded to 2.5-cm-long tabs at each end using Z-Poxy, and allowed to cure for a minimum of 24 h. For all tension tests, an 18 N load cell was used as well as an extension rate of 0.254 cm/min.

Single fiber strength is not only dependent on overall material properties, but also on the statistical flaw (defect) population along the fiber, which act essentially as local weak points [7] of the order of its diameter. Pristine filaments have a flaw population induced during manufacture, and the process of deforming the fibers induced additional flaws as discussed later. Fibers exhibit weakest-link behavior that is often well characterized by a Weibull distribution for strength, which embodies a length effect

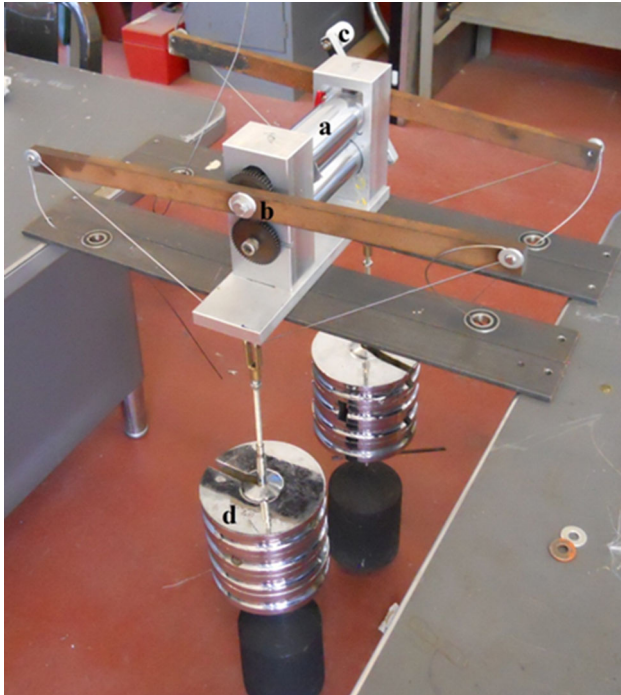


Figure 2 Device constructed to “machine” deform fibers. The machine includes chrome-coated steel rods as used in the “hand” method (a), a crank system to oppositely turn both rods (b), a manually operated handle to turn the system (c), and weights hung from the upper roller to exert a large, constant deformation force (d).

[7] (note that 1 cm of fiber consists of 588 segments or ‘links’ of length equal to the fiber diameter, D). Under the Weibull weakest-link model, the probability of failure, $P_f(\sigma)$, of a fiber of length, L , subjected to uniform stress, σ , follows

$$P_f(\sigma) = 1 - \exp \left[- \left(\frac{L}{L_0} \right) \left(\frac{\sigma}{\sigma_{L_0}} \right)^\rho \right] \\ = 1 - \exp \left[- \left(\frac{\sigma}{\sigma_L} \right)^\rho \right], \quad (2)$$

where ρ is the Weibull shape parameter, σ_{L_0} is the Weibull scale parameter corresponding to reference length, L_0 , and

$$\sigma_L = \sigma_{L_0} (L_0/L)^\rho \quad (3)$$

is the Weibull scale parameter corresponding to length L . The latter formula (3) for σ_L embodies the length effect, in that the strength decreases as the length L increases. A Weibull analysis was performed on each strength dataset, and σ_L and ρ were estimated using the method of maximum likelihood available in MATLAB.

Extensive transverse fiber deformation is likely to cause microstructural changes influencing such things as percent crystallinity and average crystallite size, which can be measured using differential scanning calorimetry (DSC). We performed DSC measurements on 1–2 mg quantities of undeformed and deformed fiber material using a TA Instruments Q20-1622, which operated over the temperature range of 30–180 °C at a ramp rate of 2 °C/min. Calibration was performed using an indium sample. The percent crystallinity, denoted X_c , can be characterized according to

$$X_c(\%) = 100 \times (\Delta H_m / \Delta H_m^0), \quad (4)$$

where $\Delta H_m^0 = 290$ J/g is the enthalpy of melting for a perfect UHMWPE crystal and ΔH_m is the melting enthalpy of the fiber calculated from the area under the melting curve [29]. Based on the work of Hoffman and Lauritzen [30, 31], the melting temperature of the semicrystalline fiber can be related to the average thickness of the crystallites by

$$d_x = \frac{2\gamma}{\Delta H_m^0} (1 - T_m/T_m^0)^{-1}, \quad (5)$$

where d_x is the average crystallite size, $\gamma = 9.3 \times 10^{-2}$ J/m² is the surface free energy of polyethylene (PE), $\Delta H_m^0 = 2.9 \times 10^8$ J/m³ is the melting enthalpy of ideal PE per unit volume, $T_m^0 = 418.95$ K is the melting temperature of an infinitely thick PE crystal, and T_m is the observed melting temperature of the fiber [29]. The values reported below are the average of at least five measurements.

Large transverse fiber deformation can also affect the fiber surface, which might alter the IFSS between the fiber and matrix. To measure the IFSS of the fibers, a single fiber pullout test was designed. Hollow polystyrene cylinders with a 3 mm diameter were cut to a length of 5 mm for undeformed fibers and 2.5 mm for deformed fibers. Single fibers were threaded into these cylinders and were placed standing on the non-adhesive side of masking tape. The cylinders were then filled with Z-Poxy and cured for 24 h. Post-cure, one end of the embedded fiber was bonded to a 2.5-cm-long tab using the same epoxy resin. The length of fiber between the cylinder and the tab was 1 cm. After a second 24-h cure, the specimens were tension tested at 1.27 mm/min until fiber slippage occurred at the polystyrene cylinder end (guaranteed by the short embedment length into the epoxy). Post-testing, the polystyrene cylinders were cut open and the exact length of epoxy

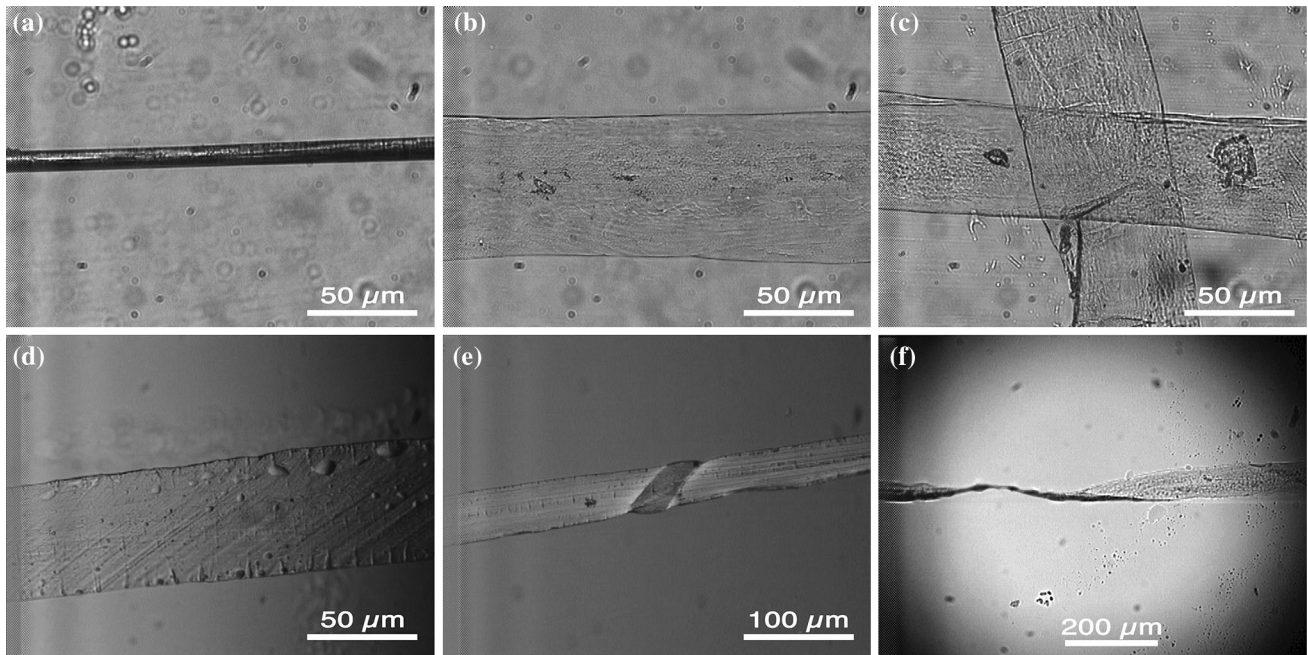


Figure 3 An undeformed UHMWPE fiber (a); a deformed fiber using the “machine” method (b); fibers are thin enough that they become optically transparent (c); the machine method often leaves edge ripple patterns and other visible surface phenomena (d); when

the machine deforms a fiber that is slightly misaligned, a kink appears that reduces fiber strength drastically (e); deformed fiber that has been twisted, to give a better sense of Φ (f).

embedding of the fiber was measured. For cylindrical fibers, the IFSS, τ_c , was estimated using

$$\tau_c = \frac{F_{p,c}}{\pi D \ell_c}, \tag{6}$$

where again D is the fiber diameter, ℓ_c is the length of cylindrical embedded fiber, and $F_{p,c}$ is the pullout force [17]. For deformed fibers in the form of micro-ribbons of rectangular cross-section, the IFSS, τ_r , was estimated using

$$\begin{aligned} \tau_r &= \frac{F_{p,r}}{2(W+h)\ell_r} \\ &= \frac{F_{p,r}}{2W(1+1/\Phi)\ell_r}, \end{aligned} \tag{7}$$

where we recall that W is the ribbon width and Φ is the cross-sectional aspect ratio, and we let ℓ_r be the embedded micro-ribbon length corresponding the pullout force $F_{p,r}$.

Results and discussion

Figure 3 shows that the transverse deformation had a drastic effect on the fiber geometry and morphology, as observed by comparing Fig. 3a with Fig. 3b, c. The

hand-deformed fibers (Fig. 3b) show few surface defects (at least over such lengths) in comparison to machine-deformed fibers (Fig. 3d), but both methods produced optically transparent fibers with height, h , less than $3 \mu\text{m}$. In the machine roll method, if the fiber axis was not exactly perpendicular to the roller axis, a fiber pulled through the machine could roll over itself, causing ‘kinks’ to appear (Fig. 3e). Fibers with such kinks were tension tested but the results were removed from the strength data, analyzed below. As expected, the machine deformation method produced a narrower distribution of fiber widths, but had a lower average aspect ratio, Φ (i.e., slightly thicker micro-ribbons). Relevant physical fiber properties are tabulated in Table 1.

The results of tension tests conducted to probe the changes in tensile strength of the fibers from before to after transverse deformation are shown in Weibull plots in Figs. 4 and 5. In calculating fiber stress, a cross-sectional area corresponding to a circular fiber with fixed diameter $D = 17.8 \mu\text{m}$ was used. A comparison of results from the two deformation methods is shown in Fig. 4, and the corresponding Weibull parameters are tabulated in Table 1. An initial comparison of σ_L values for the hand method versus

Figure 4 Comparison of the effects of hand deformation versus machine deformation on UHMWPE single fiber strength as measured at two gauge lengths. Weibull shape and scale parameters are also shown for each case.

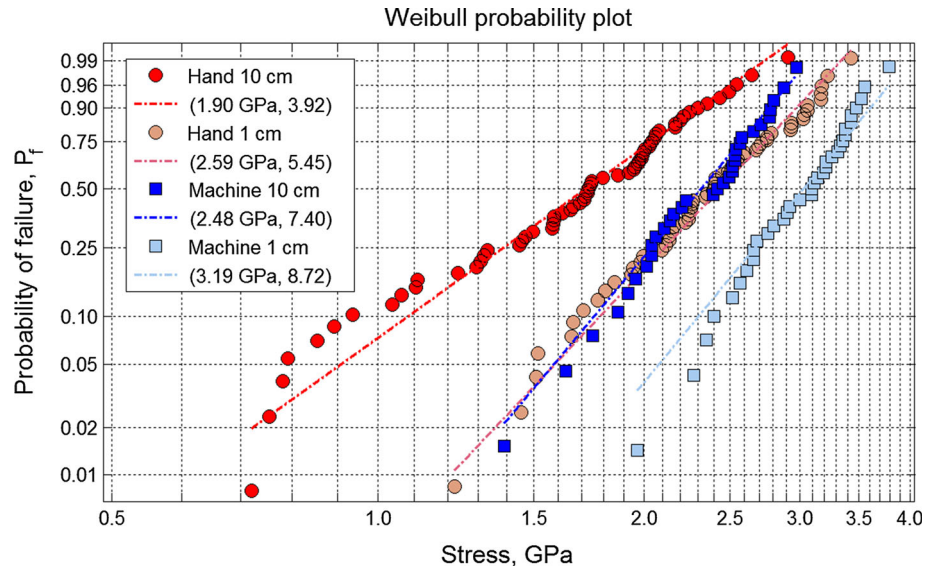
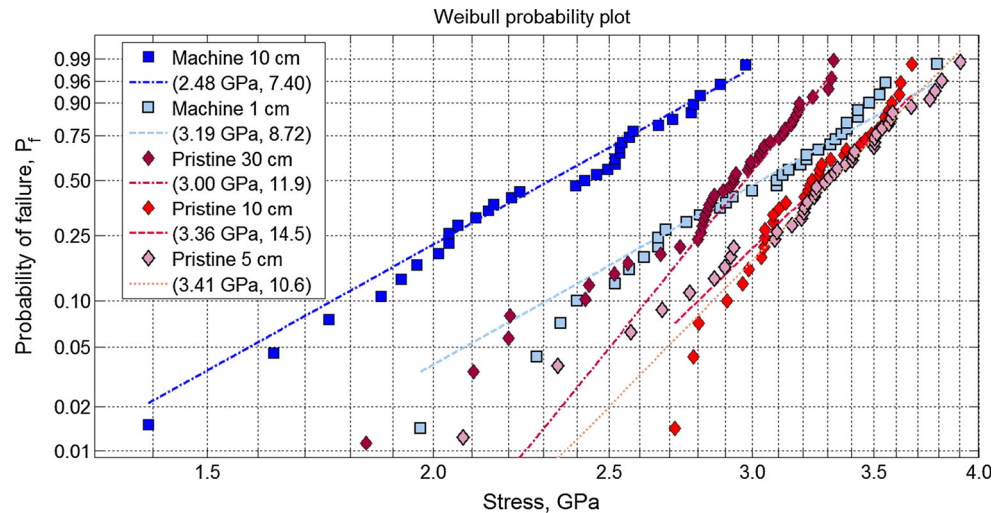


Figure 5 Comparison of machine deformation versus no deformation (pristine) on UHMWPE single fiber strength measured at various gauge lengths. Weibull shape and scale parameters are also shown.



machine roll deformation methods suggests a reduction in the fiber strength compared to pristine fibers of about 44 and 25 %, respectively. Results from specimens with gross kinks were excluded from the Weibull analysis as discussed further below. We also varied the gauge length used in our tension testing. Figure 5 also compares Weibull plots of the strengths of machine-deformed fibers at gauge lengths, L , of 1 and 10 cm to those of pristine fibers at the gauge lengths of 5, 10, and 30 cm, respectively.

It is clear from the Weibull plots in Fig. 5 that the strongest 35 % of the machine-rolled fibers (above σ_L in strength) at $L = 1$ cm are close in strength to the strongest 35 % of the pristine fibers (although admittedly at longer gauge lengths) being only about

5 % weaker. Indeed, the Weibull scale parameter values differ by only 6.5 %. This suggests that occasional random defects and flaws induced in the rolling process are responsible for significant reductions in the strengths of the specimens in which they occur. Some machine-deformed specimens, however, are relatively defect free over a 1 cm length. Thus, although the deformation process tends overall to lower the fiber strength, it does not lower it uniformly, suggesting that it may be possible to make improvements in the rolling process to greatly reduce the occurrence of such additional defects, possibly by rolling under moderate tension.

For machine-deformed fibers, flaw-induced variability in fiber strength was manifest also as a drop in the value of ρ , the Weibull shape parameter for fiber

Table 1 Various deformed and undeformed fiber properties

| Deformation method | Diameter (μm) | Height (μm) | Φ | L (cm) | σ_L (GPa) | 95 % CI (GPa) | ρ | 95 % CI |
|--------------------|----------------------------|--------------------------|--------|----------|------------------|---------------|--------|------------|
| None | 17.8 ± 1.7 | 17.8 ± 1.7 | 1 | 10 | 3.36 | 3.28–3.44 | 14.5 | 11.2–18.8 |
| Hand | 122 ± 17 | 2.0 ± 0.12 | 61 | 10 | 1.90 | 1.78–2.03 | 3.92 | 3.23–4.75 |
| Hand | 122 ± 17 | 2.0 ± 0.12 | 61 | 1 | 2.59 | 2.46–2.72 | 5.45 | 4.48–6.63 |
| Machine | 92 ± 10 | 2.7 ± 0.2 | 33 | 10 | 2.48 | 2.36–2.60 | 7.40 | 5.63–9.72 |
| Machine | 92 ± 10 | 2.7 ± 0.2 | 33 | 1 | 3.19 | 3.06–3.32 | 8.72 | 6.70–11.35 |

Weibull parameters and their confidence intervals are reported for gauge lengths of 10 cm for undeformed (pristine) fibers and for both 10 cm and 1 cm for the two deformed fiber methods. For all cases, a sample size, N , greater than 40 was used

strength, as indicated by a decrease in the slopes of the plotted data in Fig. 5. The ρ value of 10.5–14.5 for pristine fibers decreased to 7.4–8.7 for machine-deformed fibers and 4.0–5.5 for hand-deformed fibers (Fig. 4). Noting that the coefficient of variation, CV, of fiber strength (standard deviation divided by the mean) is approximately $CV \approx 1.2/\rho$, it is evident that the CV increased by about 50 percent for machine-deformed fibers and by a factor of three for hand-rolled fibers compared to pristine fibers. The defects and flaws responsible for this increased variability may have arisen from defects caused by the roll-over deformation process interacting with local inhomogeneities in the fiber material, or from roughness in the rollers and plate themselves, thus inducing small stress concentrations.

Local irregularities within the circular fibers could also become more critical weaknesses when the fiber cross-sections become highly deformed (Table 1). Such defect spreading could promote failure modes (e.g., tearing) not occurring in the original cylindrical fibers. Clearly, variability in fiber strength was magnified by the rolling process, and yet, the strongest of the deformed fiber samples were almost as strong as the strongest of the pristine fiber samples and thus were relatively flaw free. The larger ρ value of the machine deformation method, as compared to the hand deformation method, was expected, as the former process was more uniform and controlled. Nonetheless, the aspect ratio, Φ , of the hand-rolled fibers was almost double that of the machine-rolled fibers, and thus they were about 25 % thinner. This difference by itself may have accentuated the effects of inherited defects from the pristine fibers even though the fibers appeared to be smoother (Fig. 3).

Fibers with gross kinks (Fig. 3e) exhibited tensile strengths that were almost an order of magnitude lower (<500 MPa) than relatively flaw-free fibers. Such kinked fibers were easily identified in the

strength results in terms of a singular, severe flaw population, based on breaking strength alone. Weibull analysis (Fig. 4) of the strengths of the weakest sample, namely the hand-rolled, 10-cm-gauge length fibers, indicates that, in the absence of severe kinks, strengths lower than 500 MPa should occur less than 1 % of the time, and for all other stronger samples, less than 0.1 % of the time. Thus, kinks in test samples, when they occurred, had a drastic strength-reducing effect far beyond that of the other, more subtle flaws well modeled by Weibull statistics. Optical microscopy confirmed the presence of these kink defects post-testing. With further perfection of the rolling method, perhaps under mild and controlled filament tension, such kinks may possibly be avoided altogether.

To shed further light on the observed decreases in fiber strength, we also conducted DSC analysis to probe the microstructural changes in the deformed fibers (Fig. 6a). Information extracted from the thermal analysis is tabulated in Table 2. The average crystallite size was hypothesized to decrease during deformation, which correlates well with the data. Because fiber strength is believed to be controlled mainly by aligned crystals within the fibers, the 25 % drop in strength observed in tension tests matches reasonably well with the 16 % measured drop in crystallinity.

Note, however, that DSC provides information on a more “theoretical” strength limit since it is impartial to crystallite orientation. Although 80 % of the fiber remains crystalline, not all the crystalline domains will be aligned along the fiber axis after the deformation process. Therefore, the load-sharing among them will be less uniform, thus reducing the stress level triggering instability and failure [7]. Thus, strength derived solely from an X_c consideration will be overestimated.

As the fibers are being deformed, the low transverse shear modulus of PE readily allows molecular chains to slide past one another, favoring plastic

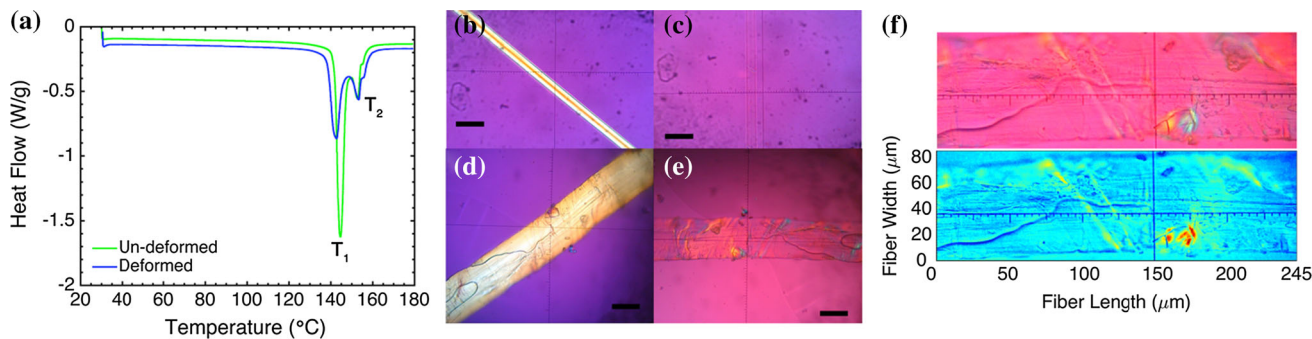


Figure 6 Typical DSC results for deformed and undeformed UHMWPE fibers (a) where T_1 corresponds to the melting temperature of orthorhombic crystals and T_2 to that for hexagonal crystals; birefringence images of undeformed fibers 45° from the extinction condition (b) and at the extinction condition (c); birefringence images of deformed fibers 45° from the extinction condition (d) and at the extinction condition (e), where misaligned

domains are clearly visible at the extinction condition only for the deformed fibers (scale bars are $50\ \mu\text{m}$); a deformed fiber (f) viewed at its extinction condition (top) and a heat map of the same image (bottom), showing the green intensity of the image. As aligned fibers disappear into the magenta background, the green intensity is a good estimate of misalignment.

deformation over fracture [25]. However, the molecular chains within UHMWPE are not free to slide, as 95 % are within crystallites [4]. It is then likely that the large deformation force caused the crystallites to break up into smaller crystalline domains. Although the DSC data indicated that crystallite size reduced from 226 to 97 nm, the absolute numbers are questionable. The suggested crystallite sizes are an order of magnitude larger than what has been observed previously for this fiber material [32, 33]. The discrepancy likely arises from the use of Eq. (5), which typically applies to crystallites with much larger lateral dimensions, i.e., in melt- or solution-crystallized chain-folded samples. Formation of crystallites in highly oriented UHMWPE fibers results in crystallites characterized by small lateral sizes [33], thus requiring a more general Gibbs–Thomson treatment as developed in recent work [34, 35]. Nonetheless, the DSC data suggest that the deformation process caused a relative decrease in crystallite size of about 60 %. When the crystallites broke down, they most likely did so along straight shear bands. Overall, the DSC data implied that the purely crystalline regions (95 % of the original fiber) broke into smaller crystallites (80 % of deformed fiber) and also amorphous regions. This resulted in a total decrease in crystallinity to 84 % of the original fibers.

Although new crystals could potentially form during the deformation process, this is unlikely due the nature of UHMWPE. The polyethylene chains are extremely inert, which makes the formation energy of

crystals very high. Because UHMWPE is gel-spun, only during drawing do enough molecular chains align to provide significant Van der Waals forces to form crystals [36]. As such, annealing of the deformed fibers showed little improvement in fiber strength. Overall, the large fiber deformation necessarily caused a decrease in percent crystallinity and crystallite size, both of which could affect the deformed fiber strength.

The rolling transverse deformation process, which likely distorted, broke down, and misaligned crystals, can then be decomposed into two potential strength degradation components: crystallinity reduction and crystal disorientation. Birefringence imaging (Fig. 6b) of the deformed fibers suggests that some crystalline regions were misaligned with the fiber axis, which perhaps provides insight into why the residual strengths of many longer deformed filaments were much less than the nominal 84 % predicted by the reduction in X_c based on DSC alone. When aligned, the crystals along the fiber axis should all have the same birefringent extinction condition and should thus disappear under the correctly polarized light. Misaligned crystallites will still be visible. Using the image's green intensity as a measure of misalignment, we find that only $\sim 2\%$ of crystallites are more than 50 % misaligned (Fig. 6c). Thus, a small population of highly misaligned crystallites could also play a significant role in the drop in observed deformed fiber strength. That said, we also note that 25 % of the machine-deformed $L = 1\ \text{cm}$ filaments had strengths very close to those of pristine filaments

Table 2 Orthorhombic crystallite melting temperature, hexagonal crystallite melting temperature, enthalpy of melting, percent crystallinity, and average crystallite thickness for deformed and undeformed UHMWPE fibers from DSC analysis

| Fiber | T ₁ (°C) | T ₂ (°C) | ΔH _m (J/g) | X _c (%) | d _x nm |
|------------|---------------------|---------------------|-----------------------|--------------------|-------------------|
| Undeformed | 144.9 ± 0.3 | 153.5 ± 0.3 | 274 ± 6 | 95 ± 2 | 225.9 ± 0.6 |
| Deformed | 143.1 ± 1.0 | 153.8 ± 0.7 | 232.2 ± 0.3 | 80.0 ± 0.1 | 95.6 ± 0.6 |

despite the fact that a gauge length of 1 cm is 110 times the width, *W*, of machine-rolled filaments. This suggests that it is possible to avoid crystallite disturbances over relatively long lengths.

While the fiber strength was statistically decreased as a result of large transverse deformation, the drastic change in geometry and surface area per unit length, as well as potential changes in micron-scale and even nano-scale surface roughness meant a potential increase in interfacial shear strength (IFSS). Using the single-fiber pullout technique described earlier in connection with (6) and (7), the pullout force, *F*_{p,r}, was measured for machine-deformed fibers, and likewise, *F*_{p,c} was measured for pristine fibers. As mentioned earlier, to generate these results the embedment length was chosen to be small enough that pullout rather than filament breakage would occur.

From these results, (7) and (6) were used to calculate the respective IFSS values, τ_r and τ_c, respectively, and the results are presented in Table 3. The IFSS of non-deformed fibers, using (6), matched very well the IFSS of the deformed fibers, using (7). This suggests that the UHMWPE fibers were drastically deformed without significantly altering the surface chemistry or roughness of the fibers. The consistency in the IFSS values strongly suggests that the observed loss in fiber strength was due to factors such as decreases in overall crystallinity within the fibers and, perhaps more significantly, to occasional local regions of misalignment of crystallites. Occasional geometric defects such as kinks, while greatly affecting fiber strength, had little effect on measured pullout loads and, thus, on IFSS.

An important quantity to consider is the ratio *l*_c/*l*_r of the lengths to achieve the same pullout force, *F*_{p,c}

or *F*_{p,r}, in the pullout experiments. Setting *F*_{p,c}/τ_c = *F*_{p,r}/τ_r, where we take τ_r = τ_c as measured, we use (6) and (7) together with (1) to arrive at

$$\frac{l_c}{l_r} = \sqrt{\frac{\Phi}{\pi}} \left(\frac{\Phi + 1}{\Phi} \right). \tag{8}$$

For machine-deformed fibers, we obtained Φ = 33, resulting in an *l*_c/*l*_r = 3.34. (For hand-rolled filaments, the corresponding result would be 4.48). This result shows that the plastic deformation that results in a large aspect ratio Φ has a major effect on the effective load transfer length needed to reload a fiber near a break, reducing this length by a factor of more than three. Various other methods involving surface treatment (e.g., by plasmas) and matrix modification have been shown to give similar increases in limiting force per unit length on circular fibers (and proportionally shorter load transfer lengths), but these use significantly more costly and involved methods [8, 9, 17–23]. These methods also report a trade-off between fiber strength and IFSS comparable to what was observed using the deformation method presented here.

This reduction in necessary stress transfer length by a factor of more than three is significant in statistical models for the strength of composites having parallel fibers in a matrix [7]. Assuming a nominal fiber strength of σ_s = 3.0 GPa and a shear stress of τ_r = τ_c ≈ 1.1 GPa, and using a force balance on a fiber segment of diameter, *D* = 17.8 μm, the critical length, *l*_s, over which the stress can be recovered to σ_s from zero at a break is given by *l*_s = (σ_s/τ_s)*D*/4, which yields *l*_s ≈ 12 mm. (This by itself indicates why gripping UHMWPE filaments is difficult, particularly

Table 3 Results from single fiber pullout tests

| Fiber | Surface area (μm) | <i>F</i> _p (mN) | IFSS (MPa) | Force/length (N/m) | Force/length increase |
|------------|-------------------|----------------------------|------------|--------------------|-----------------------|
| Undeformed | 56 ± 5 | 317 ± 63 | 1.1 ± 0.2 | 61 ± 11 | – |
| Deformed | 187 ± 19 | 500 ± 24 | 1.1 ± 0.1 | 207 ± 16 | 339 % |

Only the machine specimens were tested for the deformed fiber results. The active surface for an undeformed fiber is the circumference and for a deformed fiber it is the perimeter

in larger diameters.) For the deformed, ribbon-like fibers, this length is reduced to $\ell_s \approx 3.5$ mm, which is less than any gauge length tested. Composite strength is sensitive to this load transfer length through a factor approximately equivalent to $(\ell_c/\ell_r)^{1/\rho}$, and for the machine-deformed filaments, we obtained $\rho \approx 8$, which results in $(\ell_c/\ell_r)^{1/\rho} = 3.34^{1/8} \approx 1.16$, which corresponds to the size effect embodied in (3). This means that the reduction in strength of machine-rolled fibers compared to pristine fibers is in part potentially compensated for by a 16 % improvement in the effective strength contribution resulting from the shorter load transfer length, though this has not been not universally observed [37].

In applications requiring protection from ballistic impact, local fiber deformation (i.e., flattening) directly under the projectile contact zone plays a large role in the tension-carrying capability of the yarns required to halt the projectile in the deformation cone [2, 5]. Yarn shooting experiments reveal that the effective tensile strength of yarns is of the order $\frac{1}{2}$ of the nominal yarn tensile strength (and fiber strength) from standard tension testing [6], and this, in part, is believed to be due to local interference effects from fiber flattening in the impact zone but not right outside it, thus resulting in uneven fiber loading in the yarn. Thus, uniform pre-flattening of the fibers could prove advantageous. Moreover, the new fiber cross-section would allow the volume fraction of fibers within a composite to be significantly higher. From geometric considerations alone, cylindrical fibers of equal diameter can pack at no more than 90.7 % volume fraction (hexagonal packing), but in practice it is difficult to achieve more than 85 % [10, 11, 25]. Rectangular cross-sectioned fibers have the capability of a near 100 % packing efficiency, which in principle could improve the performance of the composite, though this has yet to be demonstrated.

Conclusions

In this work, extreme transform deformation of UHMWPE fibers was studied. The deformation process caused crystallite break-up as well as disorientation, which was evidenced by a drop in fiber strength and further supported in DSC experiments. The decrease in fiber strength was as low as 6 % for short, machine-deformed fibers and as much as 45 % for long, hand-deformed fibers that had an aspect

ratio of about 60. At the same time, a decrease in crystallinity from 95 to 80 %, and a reduction in crystallite size by about a factor of two, was indicated when comparing undeformed versus deformed fibers. The variability in fiber strength was increased, which was attributed to the deformation process and the magnification of defects that occurred from a drastic decrease in fiber height, from about 18 μm down to less than 3 μm . However, the strength retention of machine-deformed fibers was still believed high enough to yield significant ballistic protection. Potential improvements in packing efficiency, resulting from their thin micro-ribbon shape, could provide further benefits in ballistic resistance. The deformed fibers, due to their greatly increased surface area, also showed more than a factor of three decrease in the necessary load transfer length to reload a fiber near a break, which is on par with surface modification techniques on undeformed fibers. These effects are worthy of further study in ballistic protection applications.

Acknowledgements

KG acknowledges the support from the undergraduate research fund of the Department of Materials Science and Engineering at Cornell University. SLP acknowledges the financial support under the National Institute of Standards and Technology under agreement ID 70NANB14H323.

References

- [1] Cunniff PM (1999) Dimensional parameters for optimization of textile-based body armor systems, Proceedings of 18th International Symposium of Ballistics, San Antonio, TX, pp 1303–1310
- [2] Phoenix SL, Porwal PK (2003) A new membrane model for the ballistic impact response and V50 performance of multiply fibrous systems. *Int J Solids Struct* 40:6723–6765
- [3] Marissen R (2011) Design with ultra-strong polyethylene fibers. *Mater Sci Appl* 2:319–330. doi:10.4236/msa.2011.25042
- [4] Afshari M, Sikkema DJ, Lee K, Bogle M (2008) High performance fibers based on rigid and flexible polymer fibers. *Polym Rev* 48:230–274. doi:10.1080/15583720802020129
- [5] Phoenix SL, Yavuz AK, Porwal PK (2010) New interference approach for ballistic impact into stacked flexible composite body armor. *AIAA J* 48:490–501

- [6] Phoenix SL, Heisserer U, van der Werff H, van der Jagt-Deutekom MJ (2016) Modeling and experiments on ballistic impact into UHMWPE yarns using flat and saddle-nosed projectiles, submitted
- [7] Phoenix SL, Beyerlein IJ (2000) Statistical strength theory for fibrous composite materials, Chapter 1.19, in Vol. 1 of comprehensive composite materials, (6 volumes), (A. Kelly and C. Zweben, editors-in-chief; T.W. Chou, Volume 1 ed.) Pergamon (Elsevier Science)
- [8] Li ZF, Netravali AN, Sachse W (1992) Ammonia plasma treatment of ultra-high strength polyethylene fibres for improved adhesion to epoxy resin. *J Mater Sci* 48:4625–4632
- [9] Li ZF, Netravali AN (1992) Surface modification of UHSPE fibers through allylamine plasma deposition 2. Effect on fiber and fiber epoxy interface. *J Appl Polym Sci* 44:333–346
- [10] Karthikeyan K, Russell BP (2014) Polyethylene ballistic laminates: failure mechanics and interface effect. *Mater Des* 63:115–125
- [11] Attwood JP, Khaderi SN, Karthikeyan K, Fleck NA, O'Masta MR, Wadley HNG, Deshpande VS (2014) The out-of-plane compressive response of Dyneema composites. *J Mech Phys Solids* 70:200–226
- [12] ASTM-C-1557-03 (2008) Standard test method for tensile strength and young's modulus of fibers. ASTM International, West Conshohocken, PA. doi:10.1520/c1557-03r08
- [13] Hudspeth M, Nie X, Chen W (2012) Dynamic failure of Dyneema SK76 single fibers under biaxial shear/tension. *Polymer* 53:5568–5574. doi:10.1016/j.polymer.2012.09.020
- [14] Kim JH, Heckert NA, Leigh SD, Kobayashi H, McDonough WG, Rice KD, Holmes GA (2013) Effects of fiber gripping methods on the single fiber tensile test: I. Non-parametric statistical analysis. *J Mater Sci* 48:3623–3673. doi:10.1007/s10853-013-7142-y
- [15] Kim JH, Heckert NA, Mates SP, Seppala JE, McDonough WG, Davis CS, Rice KD, Holmes GA (2015) Effect of fiber gripping method on the single fiber tensile test: II. Comparison of fiber gripping materials and loading rates. *J Mater Sci* 50:2049–2060. doi:10.1007/s10853-014-8736-8
- [16] Brett Sanborn B, DiLeonardi AM, Weerasooriya T (2015) Tensile properties of Dyneema SK76 single fibers at multiple loading rates using a direct gripping method. *J Dyn Behav Mater* 1:4–14. doi:10.1007/s40870-014-0001-3
- [17] Netravali AN, Caceres JM, Thompson MO, Renk TJ (1999) Surface modification of ultra-high strength polyethylene fibers for enhanced adhesion to epoxy resins using intense pulsed high-power ion beam. *J Adhes Sci Technol* 13:1331–1342
- [18] Song Q, Netravali AN (1998) Excimer laser surface modification of ultra-high-strength polyethylene fibers for advanced adhesion with epoxy resins. Part 1: effect of laser operating parameters. *J Adhes Sci Technol* 12:957–982
- [19] Song Q, Netravali AN (1998) Excimer laser surface modification of ultra-high-strength polyethylene fibers for advanced adhesion with epoxy resins. Part 2: effect of treatment environment. *J Adhes Sci Technol* 12:983–998
- [20] Lin SP, Han JN, Yeh JT, Chang FC, Hsieh KH (2007) Surface modification and physical properties of various UHMWPE fiber reinforced modified epoxy composites. *J Appl Polym Sci* 104:655–665. doi:10.1002/app.25735
- [21] Netravali AN, Bahners T (2010) Adhesion promotion in fibers and textiles using photonic surface modification. *J Adhes Sci Technol* 24:45–75
- [22] Zhang X, Wang Y, Lu C, Cheng S (2011) Interfacial adhesion study of UHMWPE fiber-reinforced composites. *Polym Bull* 67:527–540. doi:10.1007/s00289-011-0491-2
- [23] Jin X, Wang W, Bian L, Xiao C, Zheng G, Zhou C (2011) The effect of polypyrrole coatings on the adhesion and structure properties of UHMWPE fiber. *Synt Met* 161:984–989
- [24] Hine PJ, Ward IM, Jordan ND, Olley RH, Bassett DC (2001) A comparison of the hot-compaction behavior of oriented, high-modulus, polyethylene fibers and tapes. *J Macromol Sci Phys B* 40:959–989
- [25] Russell BP, Karthikeyan K, Deshpande VS, Fleck NA (2013) The high strain rate response of ultra high molecular weight polyethylene: from fibre to laminate. *Int J Impact Eng* 60:1–9. doi:10.1016/j.ijimpeng.2013.03.010
- [26] Phoenix SL, Skelton J (1974) Transverse compressive moduli and yield behavior of some orthotropic high modulus filaments. *Text Res J* 44:934–940
- [27] Lim J, Zheng JQ, Masters K, Chen WNW (2011) Effects of gage length, loading rates, and damage on the strength of PPTA fibers. *Int J Impact Eng* 38:219–227. doi:10.1016/j.ijimpeng.2010.11.009
- [28] Marinescu A, Benea B, Pruteanu M (2006) Lapping of brittle materials, Ch4. In: IOAN D, Marinescu D (eds) Handbook of lapping and polishing. CRC Press, Boca Raton. doi:10.1201/9781420017632.ch4
- [29] Reggiani M, Tinti A, Taddei P, Visentin M, Stea S, De Clerico M, Fagnano C (2006) Phase transformation in explanted highly crystalline UHMWPE acetabular cups and debris after in vivo wear. *J Mol Struct* 785:98–105
- [30] Hoffman JD, Lauritzen JI (1961) Crystallization of bulk polymers with chain folding: theory of growth of lamellar spherulites. *J Res Natl Bur Stand* 65A:297–336
- [31] Hoffman JD, Davis GT, Lauritzen JI (1978). In: Hannary NB (ed) Treatise on solid state chemistry, vol. 3. Plenum Press, New York
- [32] Smith P, Lemstra PJ, Booij HC (1981) Ultradrawing of high-molecular-weight polyethylene cast from solution. II.

- Influence of initial polymer concentration. *J Polym Sci B Polym Phys* 19:877–888. doi:[10.1002/pol.1981.180190514](https://doi.org/10.1002/pol.1981.180190514)
- [33] Berger L, Kausch HH, Plummer CJG (2003) Structure and deformation mechanisms in UHMWPE-fibres. *Polymer* 44:5884–5887. doi:[10.1016/S0032-3861\(03\)00536-6](https://doi.org/10.1016/S0032-3861(03)00536-6)
- [34] Lippits DR, Rastogi S, Hohne SGW (2006) Melting kinetics in polymers. *Phys Rev Lett* 96:218303. doi:[10.1103/PhysRevLett.96.218303](https://doi.org/10.1103/PhysRevLett.96.218303)
- [35] Lippits DR, Rastogi S, Hohne GWH, Mezari B, Magusin PCMM (2007) Heterogeneous distribution of entanglements in the polymer melt and its influence on crystallization. *Macromolecules* 40:1004–1010. doi:[10.1021/ma0622837](https://doi.org/10.1021/ma0622837)
- [36] Yeh J-T, Lin S-C, Tu C-W, Hsie K-H, Chang F-C (2008) Investigation of the drawing mechanism of UHMWPE fibers. *J Mater Sci* 43:4892–4900
- [37] Schwartz P, Netravali A, Sembach S (1986) Effects of strain rate and gauge length on the failure of ultrahigh strength polyethylene. *Text Res J* 56(8):502–508. doi:[10.1177/004051758605600807](https://doi.org/10.1177/004051758605600807)